Supporting Information

Experimental section

Chemicals. Bismuth nitrate pentahydrate was purchased from Riedel-de Haen (Seelze, Germany). Calcium chloride, magnesium chloride, potassium chloride, sodium chloride, tris(hydroxymethyl)aminomethane (Tris), sodium phosphate tribasic, sodium phosphate dibasic, sodium phosphate monobasic, phosphoric acid, and trisodium citrate were purchased from Mallinckrodt Baker (Phillipsburg, NJ, USA). Horseradish peroxidase (HRP), human α-thrombin (~1000 NIH units/mg protein), fibrinogen (Fib), bovine serum albumin (BSA), heparin ammonium salt (1134.928 $gmol^{-1}$, from porcine intestinal mucosa, 140 USP units/mg), argatroban, and hirudin were obtained from Sigma (St. Louis, MO, USA). Warfarin was purchased from Fluka (St. Louis, MO, USA). Huamn antithrombin III (AT III) was purchased from MP Biomedicals (California, USA). Thrombin-binding aptamers (TBAs), TBA_{15} (GGT TGG TGT GGT TGG), TBA_{24} (CTA CTG GGT GGT GAG GTT GGG TAG), and TBA_{29} (AGT CCG TGG TAG GGC AGG TTG GGG TGA CT) were purchased from Integrated DNA Technologies (Coralville, IA, USA). Boric acid, hydrochloric acid, dimethyl sulfoxide (DMSO), and other metallic salts used in this study were purchased from Aldrich (Milwaukee, WI). Sodium hydroxide was purchased from Fisher Scientific (Waltham, MA, USA). Hydrogen tetrachloroaurate(III) trihydrate was purchased from Acros (Geel, Belgium). Amplex Red (AR) was purchased from Invitrogen (Carlsbad, CA, USA). Hydrogen peroxide was purchased from SHOWA (Tokyo, Japan). Milli-Q ultrapure water was used in each experiment. The buffer was 50 mM Tris-borate solution (pH 7.0, adjusted with 400 mM boric acid).

Preparation of 13-nm spherical Au NPs. The 13 nm spherical Au NPs were prepared through citrate-mediated reduction of $HAuCl_4$.[1] Aqueous 4.0 mM trisodium citrate (50 mL) was brought to a vigorous boil while stirring in a round-bottom flask fitted with a reflux condenser; 1.0 mM $HAuCl_4$ (0.5 mL) was added rapidly to the solution, which was heated for another 8 min, during which time its color changed from pale yellow to deep red. The solution was cooled to room temperature with continuous stirring. The sizes of the Au NPs were verified through transmission electron microscope (TEM) analysis (H7100, Hitachi High-Technologies Corporation, Tokyo, Japan); they appeared to be nearly monodisperse, with an average size of

13.3 ± 1.2 nm. A double-beam UV–Vis spectrophotometer (Cintra 10e, GBC, Victoria, Australia) was used to measure the absorption of the Au NP solution. The particle concentration of the Au NPs (15 nM) was determined according to Beer's law using an extinction coefficient of ca. 2.43×10^8 M^{-1} cm^{-1} at 520 nm for the 13.3-nm Au NPs.

Preparation of Bi–Au NPs. To prepare a Bi–Au NPs stock solution, a mixture of the prepared 13 nm Au NPs (15 nM, 2 mL) and Bi^{3+} ions solution (100 μM, 4 mL) was kept in Tris-borate buffer (50 mM, 4 mL, pH 7) at room temperature for 30 min. Bi^{3+} ions readily conjugated to the Au NPs through self-deposition. Using TEM analysis, we estimated the size of the Bi–Au NPs assemblies to be 13.3 (±1.7) nm (n = 5), respectively. There was no statistical difference in the average particle diameter or size distribution increases in the mean size of Bi–Au NPs, as determined from the TEM images, which suggested that there is only a monolayer or submonolayer of Bi on the surface of Au NPs. The Bi–Au NPs were stable (no aggregation) for at least one week. The as-prepared Bi–Au NPs were used in the catalytic reaction without any purification. The catalytic activity and stability of the Bi–Au NPs decreased if purification was conducted through centrifugation/wash process. We note some free Bi ions were required for providing high catalytic activity.

Characterization of Bi–Au NPs. TEM images of Bi–Au NPs were captured on an H7100 TEM (operating at 125 kV). Samples for TEM measurements were prepared by placing 20 μL of the Bi–Au NPs solution on a carbon-coated copper grid and then drying at room temperature. For surface-assisted laser desorption ionization time-of-flight ionization mass spectrometry (SALDI–TOF MS) measurements, we equilibrated aliquots (1.0 mL) of the Au NPs (750 pM) in the absence and presence of Bi^{3+} ions (10 μM) for 30 min at room temperature, and then subjected the systems to centrifugation at RCF 35,000 g for 20 min. After removing the supernatants, the precipitates were washed with water. After three centrifugation–washing cycles, the pellets were resuspended in water. A portion of the samples (1.0 μL) was placed on a stainless-steel 96-well MALDI plate and then dried at room temperature. After drying, SALDI-TOF MS measurements (Autoflex III MALDI-TOF mass spectrometer, Bruker Daltonics, Bremen, Germany) were performed on the samples. The samples were irradiated with an Nd:YAG (output: 355 nm) at 10 Hz. Ions produced by laser desorption were stabilized energetically during a delayed extraction period of 200 ns and then accelerated through the TOF system in the reflection mode prior to entering the mass analyzer. Positive ions were detected in a range from 100 to 1200 Da. To obtain high resolution and high signal-to-noise (S/N) ratios, the

laser fluence was adjusted to slightly higher than the threshold and each mass spectrum was generated by averaging 300 laser pulses.

Enzyme kinetic analysis. Kinetic measurements with AR were carried out in a black 96-well microplate using a microplate reader (Synergy 4) from BioTek (Winooski, VT, USA). AR/H_2O_2 substrate solutions in 180 μL Tris-borate solution (pH 7.0) were prepared, and the reaction was started by adding enzyme solution (20 μL) into 96-well microtiter plates. The reaction progress was monitored for 2 h, and fluorescence values of the reaction product resorufin were recorded at 585 nm by using an excitation wavelength of 540 nm, every 30 s. Variable concentrations of AR were used as substrates, while the concentration of H_2O_2 was fixed at 500 μM for Bi–Au NPs and 100 μM for HRP, respectively. Variable concentrations of H_2O_2 were used as substrates, while the concentration of AR was fixed at 10 μM. The final concentrations of the enzymes were fixed at 0.1 nM.

Procedure for comparison of stability of the Bi–Au NPs and HRP. Both Bi–Au NPs and HRP were first incubated at a range of temperatures in water baths from 20 to 80ºC (20, 40, 60, and 80ºC) or a range of pH values from 3 to 13 (3, 5, 7, 9, 11, and 13) for 2 h, respectively. Then, they were transferred to the following conditions for 2 h and their activities were measured: 5.0 mM Tris-borate solution (pH 7.0), 10 μM AR, 100 μM H_2O_2, and 750 pM Bi-Au NPs or HRP.

Bi–Au NP-based sensor for H_2O_2. For H_2O_2 sensing, aliquots (500 μL) of 5.0 mM Tris-borate solution (pH 7.0) solutions containing the Bi–Au NPs (750 pM), AR (10 μM), and H_2O_2 (0–100 μM) were equilibrated at room temperature for 1 h. The fluorescence of the resorufin (AR product) in each solution was measured using a fluorescence microplate reader (Synergy 4) from BioTek (Winooski, VT, USA), with excitation at a wavelength of 540 nm.

Preparation of Fib-Bi–Au NPs. To prepare a Fib-Bi–Au NP stock solution, a mixture of the prepared 13 nm Au NPs (15 nM, 2.0 mL) and Bi^{3+} ions solution (100 μM, 4.0 mL) was kept in Tris-borate buffer (50 mM, 4.0 mL, pH 7.0) at room temperature for 30 min. Then, Fib (5.0 μM, 8.0 mL) was added to the resulting solution. Fib molecules readily conjugated to the Bi–Au NPs through electrostatic and hydrophobic interactions.[2] From dynamic light scattering (DLS) measurements, we estimated the hydrodynamic diameters of the unlabeled Bi–Au NPs and Fib-Bi–Au NPs assemblies to be 16.3 (± 4.2) and 26.2 (±5.4) nm, respectively. The increased hydrodynamic size of the latter confirmed that fibrinogen molecules had self-assembled on the particles' surfaces. The high stability of fibrinogen-adsorbed Au NPs (Fib-Bi–Au NPs) were mainly due to the steric effect, minimizing neighboring Au NPs from getting in close enough

proximity to interact and aggregate, and high hydrophilicity of fibrinogen.[3] The steric blocking and/or electrostatic repulsion can prevent the nonspecific interaction between the Fib-Bi–Au NPs and plasma proteins.[4]

Assays of thrombin and Factor Xa activity. A series of mixtures (500 μL) of thrombin or Factor Xa (0−10 nM) and the prepared Fib-Bi–Au NPs (750 pM) in biological buffer solution (1.0X) containing plasma (10-fold dilution) were equilibrated at room temperature for 1 h. A buffer (pH 7.4) containing 25 mM Tris-HCl, 150 mM NaCl, 5 mM KCl, 1 mM $MgCl_2$, and 1 mM $CaCl_2$ was used to mimic biological conditions; for simplicity, the concentration of this biological buffer is denoted as 1X. The mixture of 800 mL biological buffer (1X) and 200 mL H_2O is denoted as 0.8X physiological buffer. Then, AR (10 μM) and H_2O_2 (50 mM) was added to the resulting solution. After reacting for 1 h at room temperature, the fluorescence of the resorufin (AR product) in each solution was measured using a fluorescence microplate reader, with excitation at a wavelength of 540 nm.

Assays of anticoagulant drugs. To screen anticoagulant drugs, aliquots (500 μL) of a solution of 5.0 mM Tris–HCl solution (pH 7.4) containing BSA (100 μM), anticoagulant drugs (500 nM), and thrombin (5 nM) in biological buffer solution (1X) were maintained at room temperature for 30 min. Then, Fib-Bi–Au NPs were added to the resulting solution at room temperature for 10 min. Finally, AR (10 μM) and H_2O_2 (50 mM) were added to the Fib-Bi–Au NPs solutions. After reacting for 1 h at room temperature, the fluorescence of the resorufin (AR product) in each solution was measured using a fluorescence microplate reader, with excitation at a wavelength of 540 nm.

Table S1. Comparison of the apparent Michaelis–Menten constant (K_M), maximal velocity (v_{max}), catalytic constant (K_{cat}), and catalytic efficiency (K_{cat}/K_M) between HRP, Bi–Au NPs, and Fib-Bi–Au NPs in the absence and presence of thrombin.

Catalyst	Substrate	K_M (μM)	v_{max} ($nM \cdot S^{-1}$)	K_{cat}[a] (S^{-1})	K_{cat}/K_M ($\mu M^{-1} \cdot S^{-1}$)
HRP	AR	94.9	27.9	279	2.93
Bi–Au NPs	AR	89.3	15.0	150	1.68
Fib-Bi–Au NPs	AR	377	1.25	12.5	0.0332
Fib-Bi–Au NPs + Thrombin (10 nM)	AR	390	0.449	4.49	0.0115
HRP	H_2O_2	7.75	1.32	13.2	1.70
Bi–Au NPs	H_2O_2	119	0.725	7.25	0.0609
Fib-Bi–Au NPs	H_2O_2	70.0	0.0344	0.344	0.00492
Fib-Bi–Au NPs + Thrombin (10 nM)	H_2O_2	64.9	0.0107	0.107	0.00165

[a] K_{cat} is the catalytic constant, where $K_{cat} = v_{max}/[E]_{total}$. $[E]_{total}$ is the molar concentration of the HRP, Bi–Au NPs or Fib-Bi–Au NPs.

The K_M value of the Bi–Au NPs with H_2O_2 as the substrate was larger than that for reported Fe_3O_4 NPs and HRP,[5] consistent with the observation that a higher concentration of H_2O_2 was required to obtain the maximal reaction velocity for Bi–Au NPs. The smooth surfaces of Bi–Au NPs have less binding sites, thus lower affinity and larger K_M values. The ionic characteristics on the surfaces of Bi–Au NPs due to adsorption of Bi^{3+}/Au^{+} ions had lower affinity toward H_2O_2 and larger K_M values. Meanwhile, with AR as the substrate, the Bi–Au NPs exhibited affinity comparable to that of HRP. The K_{cat}/K_M value gives a measure of the catalytic efficiency; an enzyme having a large value of K_{cat} (rapid turnover) or a small value of K_M (high affinity for the substrate) provides high catalyst efficiency.

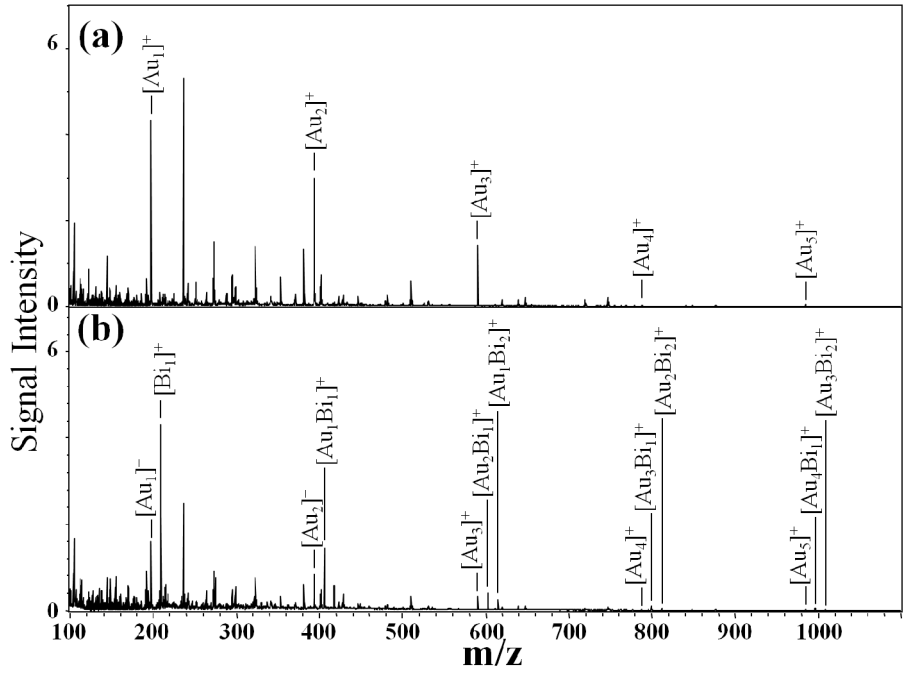

Fig. S1 SALDI-MS spectra of 5.0 mM Tris-borate solution (pH 7.0) containing Au NPs (750 pM) in the (a) absence and (b) presence of Bi^{3+} ions (10 μM). The peaks in (a) at *m*/*z* 196.97, 393.93, 590.90, 787.87, and 984.83 were assigned to $[Au_1]^+$, $[Au_2]^+$, $[Au_3]^+$, $[Au_4]^+$, and $[Au_5]^+$ ions, respectively. The peaks in (b) at *m*/*z* 208.98, 405.95, 602.91, 614.93, 799.88, 811.89, 966.85, and 1008.90 were assigned to $[Bi_1]^+$, $[Au_1Bi_1]^+$, $[Au_2Bi_1]^+$, $[Au_1Bi_2]^+$, $[Au_3Bi_1]^+$, $[Au_2Bi_2]^+$, $[Au_4Bi_1]^+$, and $[Au_3Bi_2]^+$ ions, respectively. Other conditions were as described in Fig. 1b. A total of 300 pulsed laser shots were applied under a laser fluence set at 51.25 μJ.

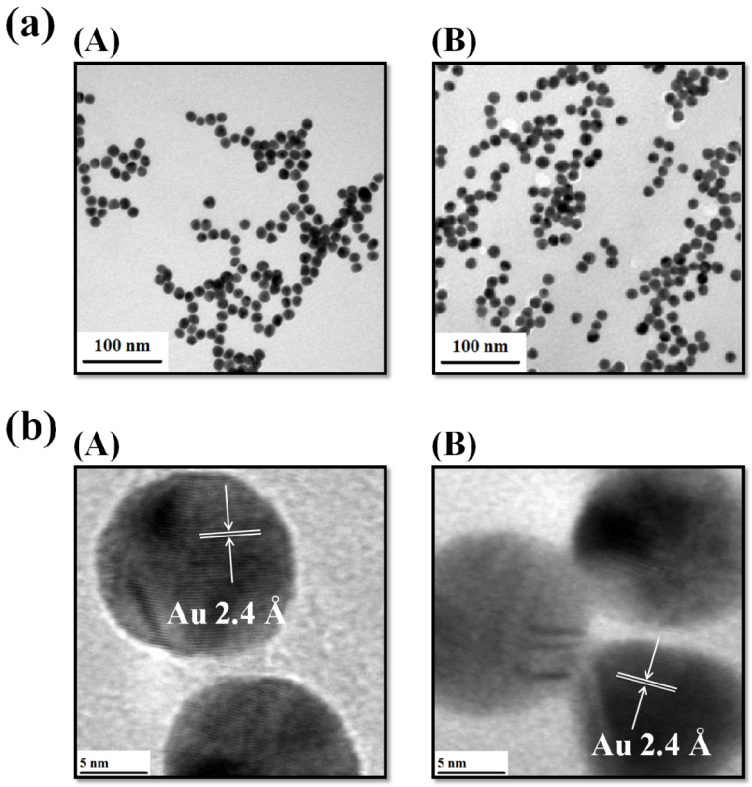

Fig. S2 (a) TEM and (b) HRTEM images of Au NPs in the (A) absence and (B) presence of Bi^{3+}. Other conditions were as described in Fig. 1b. Average Au NP sizes in Fig. S2a (A) and (B) are 13.3 ± 1.2 and 13.3 ± 1.7 nm, respectively. The lattice fringes in both (A) and (B) are consistent with metallic gold having a discerned lattice spacing of 2.4 Å, which corresponds to the d-spacing of the (111) crystal plane of face-centered cubic (fcc) Au.

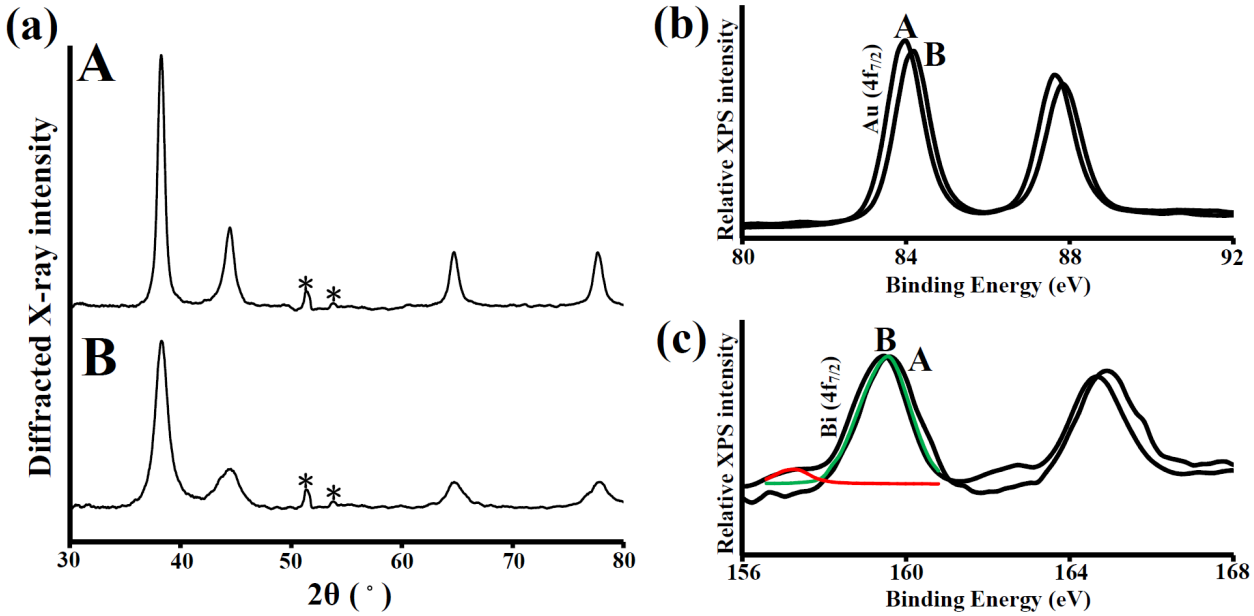

Fig. S3 (a) XRD patterns of Au NPs in the (A) absence and (B) presence of Bi^{3+}. (b) Au 4f core-level photoelectron spectra of Au NPs in the (A) absence and (B) presence of Bi^{3+} dosed onto silicon substrates and measured at room temperature. (c) Bi 4f core-level photoelectron spectra of (A) Bi^{3+} (10 μM) and (B) Bi–Au NPs (750 pM) dosed onto silicon substrates and measured at room temperature. Other conditions were as described in Fig. 1b. The XRD patterns (Fig. S3a) in both (A) and (B) show a face-centered cubic (fcc) structural characterization that exhibited diffraction peaks of (111), (200), (220), and (311) at 2θ values of 38.5, 44.7, 66.0, and 78.4, respectively. The peaks labeled with stars are assigned to the diffraction of the silicon wafer substrate. The BE (285.3 eV) of the alkyl chain C 1s orbital is given in Fig. S3b and c as an internal reference. The Bi $4f_{7/2}$ core-level photoelectron spectra of Bi–Au NPs was deconvoluted to Bi^0 (red curve) and Bi^{3+} (green curve).

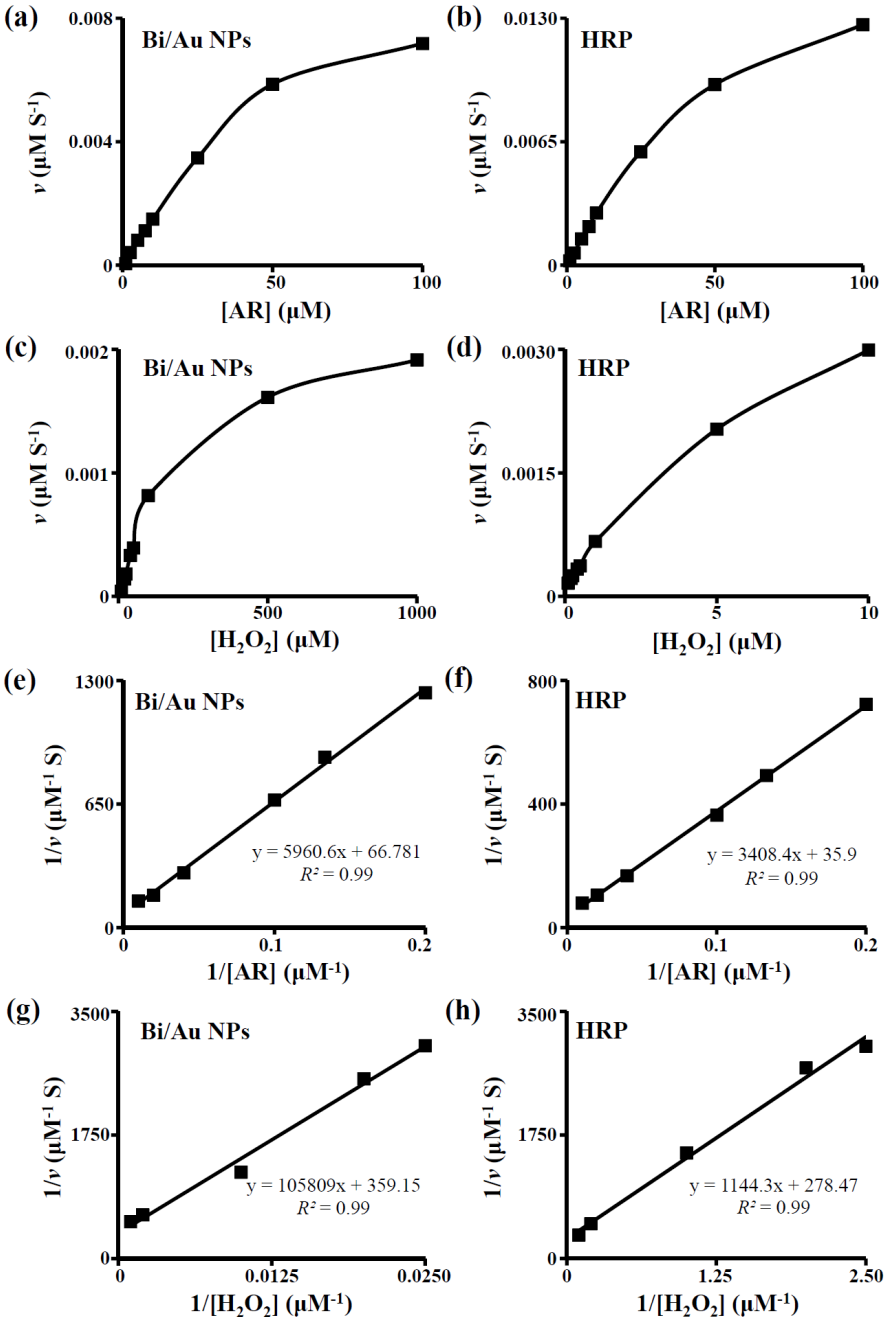

Fig. S4 Steady-state kinetic assay and catalytic mechanism of HRP and Bi–Au NPs. The velocity (v) of the reaction was measured using (a, c) 100 pM Bi–Au NPs or (b, d) 100 pM HRP in 5 mM Tris-borate (pH 7.0). (a, b) The concentration of H_2O_2 was 100 μM and 500 μM for HRP and Bi–Au NPs, respectively, and the AR concentration was varied. (c, d) The concentration of AR was 10 μM and the H_2O_2 concentration was varied. Double reciprocal plots of the activity of (e, g) Bi–Au NPs and (f, h) HRP with the concentration of one substrate (H_2O_2 or AR) fixed and the other varied.

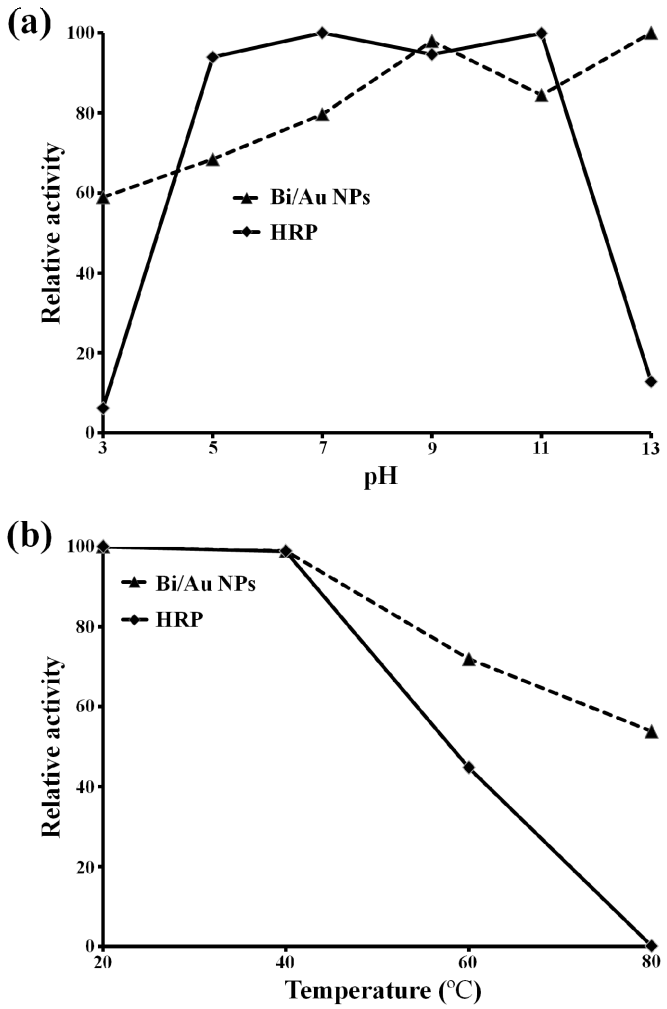

Fig. S5 Comparison of the stabilities of Bi–Au NPs and HRP. (a) Bi–Au NPs and HRP were first incubated at pH 3–13 (5 mM sodium phosphate) for 2 h, and then their peroxidase activities were measured under standard conditions (10 μM AR, 100 μM H_2O_2, 5.0 mM Tris-borate, pH 7.0, 25°C). (b) Bi–Au NPs and HRP were first incubated at 20–80°C for 2 h and then the peroxidase activity was measured under standard conditions (10 μM AR, 100 μM H_2O_2, 5 mM Tris-borate, pH 7.0, 25°C). Other conditions were as described in Fig. 1a.

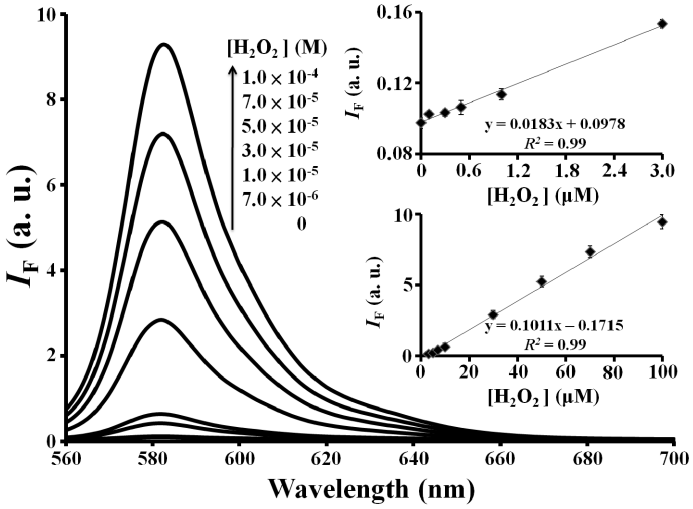

Fig. S6 Fluorescence spectra of Bi–Au NPs (750 pM) in 5.0 mM Tris-borate (pH 7.0) in the presence of AR (10 μM) and H_2O_2 (0–100 μM). Inset: Plot of the fluorescence response (I_F) at 585 nm of the AR–Bi–Au NPs for H_2O_2. Error bars in the inset represent the standard deviations from three repeated experiments. Other conditions were as described in Fig. 1a.

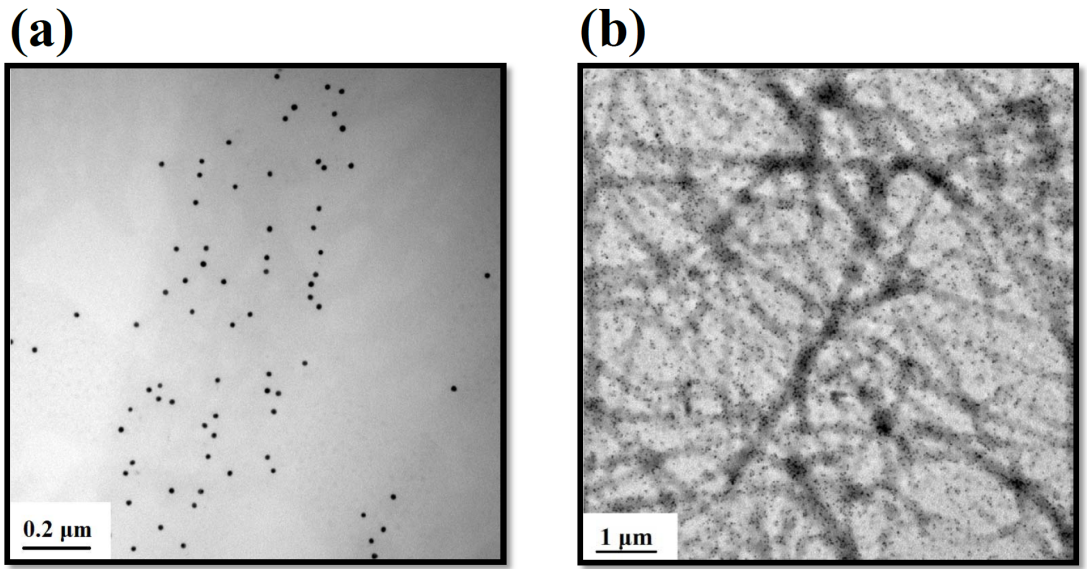

Fig. S7 TEM images of solutions containing Fib-Bi–Au NPs in the (a) absence and (b) presence (10 nM) of thrombin. Other conditions are as described in Fig. 2.

As shown in Scheme 1b, thrombin induced the formation of insoluble fibrillar fibrin from the Fib-Bi–Au NP solution in the presence of excess fibrinogen through the polymerization of unconjugated and conjugated fibrinogen. Owing to decreases in the surface area and active sites, the catalytic ability of the Fib-Bi–Au NPs toward the H_2O_2-mediated AR reaction was inhibited. In addition, decreased diffusion of AR and H_2O_2 across the Fib-Bi–Au NP surfaces in the fibrin is another contributor. Because the catalytic activity of Fib-Bi–Au NPs is strongly related to the concentration of thrombin, the fluorescence intensity of the AR product at 585 nm was used to determine the activity (concentration) of thrombin. A low fluorescence intensity value corresponds to a high degree of fibrillar fibrin on Bi–Au NPs (high enzymatic activity of thrombin).

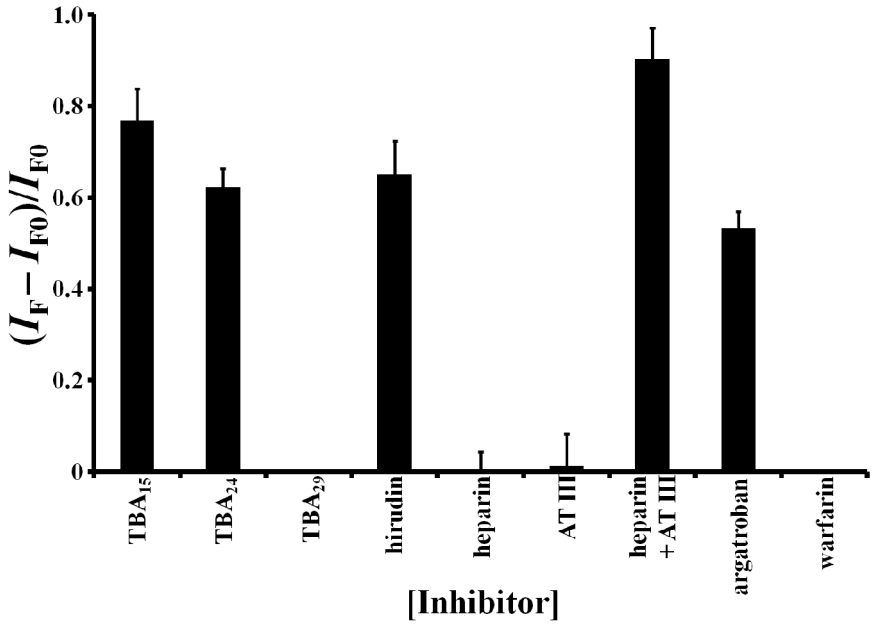

Fig. S8 Validation of the use of the thrombin AR/H_2O_2–Fib-Bi–Au NP probe to screen the inhibitor of thrombin. I_{F0} and I_F are the fluorescence intensities of the solution in the absence and presence of the anticoagulant drug, respectively. Error bars represent the standard deviations from three repeated experiments. Other conditions are as described in Fig. 2.

We tested the three best-known thrombin-binding aptamers (TBAs)—15-base-long aptamers (TBA_{15}) and 24-base-long aptamers (TBA_{24}), which bind to exosite I, and 29-base-long aptamer (TBA_{29}), which interacts with exosite II. The dissociation constants (K_d) for these interactions of thrombin with TBA_{15}, TBA_{24}, and TBA_{29} are ca. 100, 10, and 0.5 nM, respectively.[6] As shown in Fig. S8†, the activity of thrombin (5.0 nM) was suppressed to ~77% by TBA_{15} (500 nM) and ~62% by TBA_{24} (500 nM), whereas TBA_{29} exhibited no obvious anticoagulant activity. Fig. S8† also shows that the activity of thrombin (5.0 nM) was inhibited to 65% by hirudin (5 μM), which is the most-potent noncovalent inhibitor of thrombin. Hirudin is a 65-amino-acid polypeptide that inhibits thrombin by interacting simultaneously with the active site and exosite I with ultra-high affinity (K_d~10^{-14} M).[7] Fig. S8 indicates low thrombin activity in the presence of human antithrombin III (AT III) (500 nM) and heparin (500 nM), but no obvious inactivation of thrombin in the presence of either AT III or heparin. The rate of thrombin inactivation by human AT III is relatively low. After conformational change induced by heparin, AT III irreversibly binds to and inhibits the active site of thrombin.[8] The rate of AT III thrombin inactivation is accelerated 2000–4000-fold in the presence of heparin.[8] Our assay also agrees with the literature showing that argatroban is a direct thrombin inhibitor (DTI) that reversibly binds to the thrombin active site and does not require the cofactor AT III for antithrombotic activity.[9] On the other hand, our result revealed that warfarin is not a DTI; it works by suppressing the production of some clotting factors (interfering with prothrombin and factor VII activation) and thereby inhibiting blood clotting.[10] These results reveal that the AR/H_2O_2–Fib-Bi–Au NPs have high potential for screening the anticoagulant drugs of DTI.

References:

1 (*a*) J. Turkevich, P. C. Stevenson and J. Hillier, *Discuss*. *Faraday Soc*., 1951, **11**, 55–75; (*b*) B. V. Enüstün and J. Turkevich, *J*. *Am*. *Chem*. *Soc*., 1963, **85**, 3317–3328.

2 (*a*) S. H. Brewer, W. R. Glomm, M. C. Johnson, M. K. Knag and S. Franzen, *Langmuir*, 2005, **21**, 9303–9307; (*b*) K. Vangala, F. Ameer, G. Salomon, V. Le, E. Lewis, L. Y. Yu, D. Liu and D. M. Zhang, *J*. *Phys*. *Chem*., 2012, **116**, 3645–3652.

3 C.-K. Chen, C.-C. Huang and H.-T. Chang, *Biosens. Bioelectron.*, 2010, **25**, 1922–1927 .

4 A. E. Nel, L. Mädler, D. Velegol, T. Xia, E. M. V. Hoek, P. Somasundaran, F. Klaessig, V. Castranova and M. Thompson *Nature Mater.*, 2009, **8**, 543–557.

5 L. Z. Gao, J. Zhuang, L. Nie, J. B. Zhang, Y. Zhang, N. Gu, T. H. Wang, J. Feng, D. L. Yang, S. Perrett and X. Yan, *Nat*. *Nanotechnol*., 2007, **2**, 577–583.

6 (*a*) K. Padmanabhan, K. P. Padmanabhan, J. D. Ferrara, J. E. Sadler and A. Tulinsky, *J*. *Biol*. *Chem*., 1993, **268**, 17651–17654; (*b*) D. M. Tasset, M. F. Kubik and W. Steiner, *J*. *Mol*. *Biol*., 1997, **272**, 688–698.

7 T. J. Rydel, A. Tulinsky, W. Bode and R. Huber, *J*. *Mol*. *Biol*., 1991, **221**, 583–601.

8 S. T. Olson and I. Björk, *J*. *Biol*. *Chem*., 1991, **266**, 6353–6364.

9 B. E. Lewis, D. E. Wallis, S. D. Berkowitz, W. H. Matthai, J. Fareed, J. M. Walenga, J. Bartholomew, R. Sham, R. G. Lerner, Z. R. Zeigler, P. K. Rustagi, I. K. Jang, S. D. Rifkin, J. Moran, M. J. Hursting and J. G. Kelton, *Circulation*, 2001, **103**, 1838–1843.

10 J. Ansell, J. Hirsh, L. Poller, H. Bussey, A. Jacobson and E. Hylek, *Chest*, 2004, **126**, 204S–233S.